GRAPH-BASED PERMUTATION PATTERNS FOR THE ANALYSIS OF TASK-RELATED FMRI SIGNALS ON DTI NETWORKS IN MILD COGNITIVE IMPAIRMENT

John S. Fabila-Carrasco[*†], *Avalon Campbell-Cousins*[*†], *Mario A. Parra-Rodriguez*[+], *Javier Escudero*[†]

[†] School of Engineering, IDCOM, University of Edinburgh, UK
[+] Department of Psychological Sciences and Health, University of Strathclyde, UK

ABSTRACT

Permutation Entropy (PE) is a powerful nonlinear analysis technique for univariate time series. Recently, Permutation Entropy for Graph signals ($\mathrm{PE_G}$) has been proposed to extend PE to data residing on irregular domains. However, $\mathrm{PE_G}$ is limited as it provides a single value to characterise a whole graph signal. Here, we introduce a novel approach to evaluate graph signals *at the vertex level*: graph-based permutation patterns. Synthetic datasets show the efficacy of our method. We reveal that dynamics in graph signals, undetectable with $\mathrm{PE_G}$, can be discerned using our graph-based patterns. These are then validated in DTI and fMRI data acquired during a working memory task in mild cognitive impairment, where we explore functional brain signals on structural white matter networks. Our findings suggest that graph-based permutation patterns in individual brain regions change as the disease progresses, demonstrating potential as a method of analyzing graph-signals at a granular scale.

***Index Terms*—** Graph signals, Permutation entropy, Graph topology, Permutation patterns, Neuroimaging.

1. INTRODUCTION

Entropy-based nonlinear analysis techniques have become particularly valuable for analysing noisy or short time series related to complex systems [2, 25]. These methods offer insights into signal irregularity, revealing effects such as financial crisis in time series [30] and anomalies in mechanical and physiological systems [1]. Among them, permutation entropy (PE) is noted for its robustness to noise, fast calculation, and sound statistical properties [9].

Building on Shannon's entropy, PE quantifies the distribution of 'permutation patterns' in time series [4]. Such patterns have broad applications, from biomedical to finance data [26]. Advanced quantifiers further refine time series analysis, like 'forbidden patterns' in finance [32] and weighted differences of pattern likelihoods for univariate brain signals [3]. Additionally, the contrasts α (turning rate) and β (up-down balance) further refine permutation pattern analysis [3]. While PE is powerful, its univariate focus is a limitation. A multivariate PE version exists but it dilutes individual channel characteristics [18]. More recently, a 2D version of PE has been proposed for images [19].

Graph signals offer a novel avenue for data analysis on irregular domains [11, 21]. The framework of graph signals is highly relevant for a wide variety of settings, such as weather patterns or vehicular traffic [20]. One particularly relevant example is neuroimaging, where brain activity can naturally be seen as a graph signal measured over a brain network [7, 15, 17]. In this context, we have recently introduced $\mathrm{PE_G}$ for graph signals [12], extending PE to irregularly sampled data.

Permutation patterns have received considerable attention recently due to their useful properties in univariate time series, and their study has very recently been extended to 2D formulations [5]. However, they remain unexplored for graph signals. Our contributions are:

- The first definition of permutation patterns for graph signals as a way to characterise them at granular level.
- Extension of the contrasts α (turning rate) and β (up-down balance) to graph signals for detailed pattern analysis.
- The study of the behaviour of α and β for synthetic benchmarks of graph signals.
- The illustration of graph permutation patterns to characterise local changes in neuroimaging datasets in mild cognitive impairment, a prodromal phase of Alzheimer's disease.

2. GRAPH-BASED PERMUTATION PATTERNS

2.1. Notation

Let $G = (\mathcal{V}, \mathcal{E}, \mathbf{A})$ represent a *simple undirected graph* with vertex set $\mathcal{V} = \{v_1, v_2, \ldots, v_N\}$ and edge set $\mathcal{E}$ defined as $\mathcal{E} \subset \{(v_i, v_j) | v_i, v_j \in \mathcal{V}\}$. The adjacency matrix $\mathbf{A}$ is an $N \times N$ symmetric matrix with $\mathbf{A}_{ij} = 1$ if an edge connects v_i and v_j, and $\mathbf{A}_{ij} = 0$ otherwise.

*These authors share first authorship. This work was supported by the Leverhulme Trust via a Research Project Grant (RPG-2020-158) to JER and by Alzheimer's Society Grants AS-R42303 and AS-SF-14-008 awarded to MAP in collaboration with JER. ACC acknowledges Edinburgh University's Principle's Career Development PhD Scholarship and Federica Guazzo for pre-processing the fMRI data.

A *graph signal* $\mathbf{X}$ maps $\mathcal{V} \to \mathbb{R}$. $\mathbf{X} = [x_1, x_2, \ldots, x_N]^T$ is a column vector where the indices correspond to $\mathcal{V}$.

A *permutation* π is a bijection $\pi : \mathbb{N}_m \to \mathbb{N}_m$ with $\mathbb{N}_m = \{1, 2, \ldots, m\}$. Using shorthand, π_k stands for $\pi(k)$ for each $k \in \mathbb{N}_m$, and the permutation is expressed as $\pi = \pi_1\pi_2 \ldots \pi_m$. The complete set of permutation patterns is denoted by Π. For instance, the notation $\pi = 321$ implies $\pi(1) = 3$, $\pi(2) = 2$, and $\pi(3) = 1$. Given a vector $\mathbf{x} = (x_1, x_2, \ldots, x_m) \in \mathbb{R}^m$, $\mathbf{x}$ is said to exhibit the pattern π if $\pi_i < \pi_j$ is true if and only if $x_i < x_j$. Lastly, $|\cdot|$ denotes cardinality.

2.2. Graph-based permutation patterns

Let $\mathbf{X}$ be a graph signal defined on G, and $2 \leq m \in \mathbb{N}$ be the *embedding dimension*. The graph-based permutation patterns are defined as follows:

1. The *embedding matrix* $\mathbf{Y} \in \mathbb{R}^{N\times m}$ is given by $\mathbf{Y} = [\mathbf{y}_0, \mathbf{y}_1, \cdots, \mathbf{y}_{m-1}]$, defined by
$$\mathbf{y}_k = D^k\mathbf{A}^k\mathbf{X} \in \mathbb{R}^{N\times 1}\ , \quad k = 0, 1, \ldots, m-1\ , \quad (1)$$
where D^k is the diagonal matrix $D^k_{ii} = 1/\sum_{j=1}^{N}(\mathbf{A}^k)_{ij}$.
2. *Graph-based permutation patterns.* Each vertex of the graph is assigned an *embedding vector* and mapped to a unique permutation pattern. Formally, the *embedding vectors* consist of m numbers corresponding to each row of the matrix $\mathbf{Y}$, i.e., $\mathrm{row}_i(\mathbf{Y}) = (y_{ij})_{j=1}^{m}$ for $i = 1, 2, \ldots, N$. Each embedding vector (one for each vertex of the graph) is uniquely mapped to a permutation pattern, i.e., $v_i \to \mathrm{row}_i(\mathbf{Y}) \to \pi \in \Pi$.
3. *Relative frequencies.* For each dispersion pattern $\pi \in \Pi$, its relative frequency, $\rho(\pi) \in [0, 1]$, is obtained as:
$$\rho(\pi) = |\{v_i \mid v_i \in \mathcal{V} \text{ and } v_i \text{ has type } \pi\}|/N. \quad (2)$$

2.3. Permutation patterns and contrast for length 3

Here, we focus on $m = 3$ (depicted in Fig. 1), which is a well-studied case in univariate time series [3]. Increased pattern lengths make statistical estimates of pattern frequencies less accurate and their interpretation increasingly challenging [3].

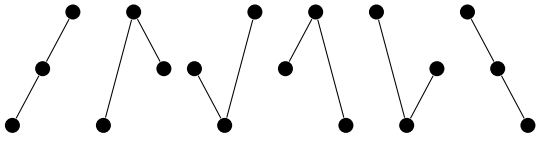

(a) 123 **(b)** 132 **(c)** 213 **(d)** 231 **(e)** 312 **(f)** 321

Fig. 1: The six permutation patterns for $m = 3$

The turning rate, denoted as α, quantifies the prevalence of turning points relative to monotonically increasing or decreasing segments within a time series. The up-down balance, denoted as β, distinguishes upward and downward patterns [3]. They are traditionally defined as:

$$\alpha = \rho(132) + \rho(213) + \rho(231) + \rho(312)\ ; \quad (3)$$
$$\beta = \rho(123) - \rho(321)\ . \quad (4)$$

As detailed in Sec. 2.2, we can expand the traditional definitions of α and β beyond their original scope in [3]. Notably, the graph signal contrast matches that of a univariate time series when the graph is a directed path. However, our graph-based approach allows us to craft more encompassing contrasts, integrating both graph's topology and data.

A critical nuance of our methodology is its ability to assign a distinct pattern to each sample. This contrasts with time series permutation patterns. This granularity affords deeper insights into graph signals, enabling precise characterization of each data point.

3. BENCHMARKING ON SYNTHETIC DATA

MIX **Processing.** In a *Random Geometric Graph* (RGG), each vertex $v_i \in \mathcal{V}$ is assigned a random 2D coordinate $\mathbf{z}_i = (z_i^1, z_i^2) \in [0, 1]^2$. Vertices v_i and v_j, are connected if their coordinates' distance is $\leq r$. For vertex v_i, the signal value is determined by:

$$\mathrm{MIX}(v_i) = ((1 - R)S(\mathbf{z}_i) + RW(\mathbf{z}_i))\,, 1 \leq i \leq N\ . \quad (5)$$

Here, R is a random variable with a probability p of being 1 and $1 - p$ of being 0, W represents uniformly distributed white noise, and $S(\mathbf{z_i}) = \sin(2\pi f z_i^1) + \sin(2\pi f z_i^2)$. For $p = 0$, $\mathrm{MIX}(v_i) = S(\mathbf{z}_i)$, which is a regular periodic signal and for $p = 1$, MIX is entirely noise, allowing exploration of both structured and stochastic graph behaviors as in [13].

Permutation Entropy Analysis. Our investigation centered on discerning the irregularities of the MIX graph signal, especially those affected by the variations in parameters f and p. Throughout this process, the RGG parameters remained constant at $N = 1500$ and $r = 0.06$, and the study spanned 20 realizations. The initial step involved computing the entropy – $\mathrm{PE_G}$ – for the graph signal values. The resulting entropy mean and standard deviation (std), evaluated across different MIX process frequencies, are presented in Fig. 2. Our observations indicate that relying purely on the permutation entropy value falls short in delivering clear insights. Specifically, this method does not effectively track the signal dynamics amid rising noise or shifting frequency.

Permutation Pattern Analysis Using our graph-based permutation pattern analysis, we present an exploration of the MIX process.

Baseline Behavior at $p = 0$: At this level, the MIX signal naturally shows periodic tendencies. When the frequency increases, α slightly drops due to fewer local extrema. As expected, $\beta \approx 0$ because the MIX signal for $p = 0$ is governed by the sinusoidal components, resulting in a similar number of monotonically increasing and decreasing patterns.

Effects of Noise and p: An increase in noise or the p parameter leads to a rise in α, reflecting a decrease in the num-

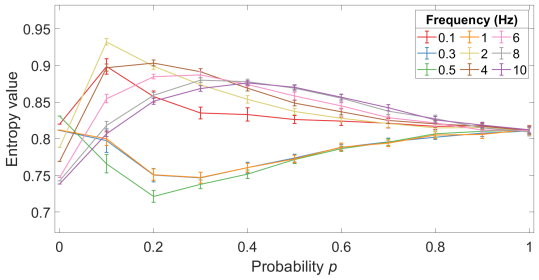

Fig. 2: Mean and std of values of $\mathrm{PE_G}$ for a consistent graph across increasing noise levels and varying frequencies.

ber of strictly monotonous patterns. Notably, a slight change in p from 0 to 0.1 causes a significant increase in α. This underscores the MIX process's sensitivity to small changes, with the trend stabilizing for higher p values, as illustrated in Fig. 3(a). The interplay between the noise and period of the sinusoids results in values of β deviating from 0.

Frequency Relationship: Notably, for a constant p, α shows a direct relationship with frequency: a decrease in frequency leads to a heightened α. Conversely, higher frequencies result in fewer local points, leading to a reduced α.

Increases in r augments graph connectivity, thereby enhancing sensitivity to frequency changes.

The β-α Complementarity: α and β display different behaviours, confirming that they both provide complementary information, as shown in Fig. 3.

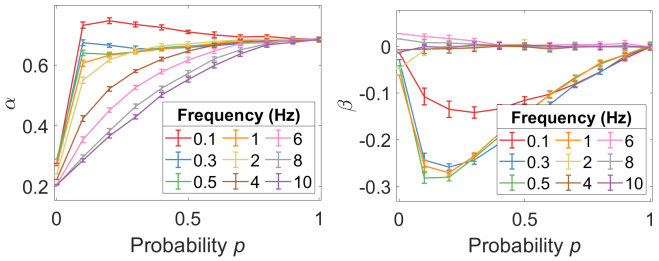

(a) Turning rate α (b) Up-down balance β

Fig. 3: Graph-based contrasts for the MIX process.

4. REAL-WORLD ILLUSTRATION IN MCI

Dementia currently affects over 50 million people worldwide and is expected to triple by 2050 [27]. Alzheimer's disease (AD) is the main cause of dementia and causes immense emotional and financial strain on families and healthcare services. Its early stages are often categorized by stages of Mild Cognitive Impairment (MCI), often progressing (within 4 years) to the dementia stage of AD [27]. To understand this progression, we explore a novel MRI model of AD and its potential use in characterizing the stages of disease.

4.1. Participants and task

Participants from the longitudinal study [23] were assessed with a battery of neuropsychological tests commonly used to assess dementia, grouping subjects into early Mild Cognitive Impairment (eMCI), MCI, and Alzheimer's disease converters after a 2-year follow up (MCIc) [23]. From these, 8 healthy controls (Age: 76.50 ± 5.21, Sex: 2M; 6F), 7 eMCI (Age: 76.86 ± 6.41, Sex: 4M; 3F), 10 MCI (Age: 72.30 ± 5.64, Sex: 5M; 5F), and 6 MCIc subjects (Age: 76.33 ± 5.09, Sex: 4M; 2F) were selected to undergo DTI and fMRI acquisition during which they performed a Visual Short-Term Memory Binding Task (VSTMBT).

The VSTMBT [22] is a task sensitive to memory related changes in early stage AD. Participants were presented non-nameable coloured shapes on a screen for 2s (encoding). They must memorize this information after a blank screen is shown for a variable amount of time of 2, 4, 6, or 8s (maintenance). Then, they are presented the same or a different set of associations of shapes and colours for 4s. The participants must determine if they are the same or different (probe), followed by an inter-trial interval before repetition. In this study, we focus on the encoding phase of the task to assess the formation of memories in healthy and diseased groups.

4.2. Graph and signal construction

fMRI data was collected with a GE Signa Horizon HDxt 1.5T clinical scanner. During the VSTMBT, contiguous interleaved axial gradient EPI were collected alongside the intercommissural plane throughout two continuous runs (TR/TE $=$ 2000/40ms; matrix $=$ 64×64; fov $=$ 24cm; thickness $=$ 5mm; gap $=$ 0mm).

Outlier detection, realignment, slice-timing correction, co-registration of the structural (T_1) and functional images to the MNI space, segmentation, and normalization were performed with SPM12. ROIs for each subject are defined using an 85 region atlas, detailed below. For each ROI, the mean signal is acquired across the voxels in that region and highpass filtered (0.06Hz) to avoid fMRI signal drift.

For Diffusion MRI, 3 T_2-weighted (b $=$ 0s mm^{-2}) and sets of diffusion-weighted (b $=$ 1000s mm^{-2}) single-shot spin-echo-planar (EP) volumes were acquired with diffusion gradients applied in 32 non-collinear directions. Subsequent volumes were in the axial plane (fov $=$ 240×240; matrix $=$ 128×128; thickness $=$ 2.5mm), giving voxel dimensions of $1.875 \times 1.875 \times 2.5$mm.

A T_1 weighted volume was also acquired with 1.3 mm^3 voxel dimensions. This volume was parcellated into 85 ROIs with the Desikan-Killiany atlas combined with additional regions acquired via sub-cortical segmentation detailed in [8], and the brain-stem using FreeSurfer. Standard pre-processing was applied following [8], resulting in DTI networks where edge weight was determined by the streamline density (SD) between regions, corrected for ROI size.

4.3. Results

We calculate the graph-based patterns as per Sec. 2.2 with $m = 3$. The graph is the subject's SD-weighted DTI network and the signal *at each node* is the mean signal across the encoding phases of the task, yielding a pattern at each node. Though limited by sample size, in the healthy brain networks, we observe the existence of dominant patterns in some clusters, such as patterns 5&6 in ROIs 1-18, and patterns 1&2 in ROIs 75-81 (see Fig. 4a), suggesting that there may be some identifying patterns associated with the encoding phase of the VSTMBT. (Here we refer to patterns #1 to #6 following the order as in Fig. 1.)

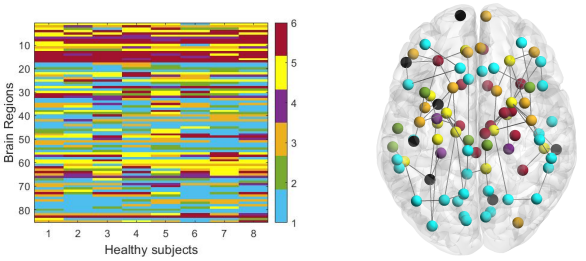

(a) Patterns across subjects (b) Brain visualization

Fig. 4: (a) visualizes the distribution of patterns (rows), across subjects (columns). In (b), patterns for a node were based on the mode of the distribution of patterns for the healthy group, but only when that pattern was in at least half of subjects (black otherwise). (b) was generated with the BrainNet viewer tool [29].

To determine whether patterns change with disease, we perform chi-squared analysis comparing the per node patterns between each pair of control and disease groups. Furthermore, we assess the stability of the resulting p-value by permuting the control and disease groups 1000 times to calculate how often our original p-value (p) is smaller than that of the randomly permuted groups (p'). Due to the limited sample size, we took a conservative approach to report regions where both $p, p' \leq 0.05$.

Control vs.	**ROIs**	p**-value**	$p < p'$
eMCI	Right-lateralorbitofrontal	0.019	0.009
MCI	Right-entorhinal	0.015	0.002
	Right-lateralorbitofrontal	0.020	0.027
	Right-parahippocampal	0.010	0
MCIc	Left-hippocampus	0.049	0.050
	Left-caudalmiddlefrontal	0.036	0.033
	Left-medialorbitofrontal	0.031	0.008
	Right-lateralorbitofrontal	0.005	0
	Right-paracentral	0.049	0.021

Table 1: Statistical tests to find regions with significant differences in the distribution of graph-based permutation patterns between control and different stages of MCI.

We find that, as the disease progresses (Table 1), the number of regions which exhibit a significant change in pattern increases, following a neuroanatomical trajectory consistent with that described by the AD continuum, i.e., Medial Temporal Lobe (MTL) regions first and then broader impact including frontal lobes [6, 10, 23]. Not only was the gross neuroanatomical spread of AD pathology found, but our method identified the more fine grained distribution of pathology within the MTL characterizing the earliest stages of AD (i.e., entorhinal which feeds to parahippocampal and hippocampal regions [6, 10, 23]). Specifically, we see an increasing change in the orbitofrontal cortex as the disease progresses both with decreasing p-value in the Right lateral orbitofrontal, along with the presence of the medial orbitofrontal at the later stage of disease. The orbitofrontal cortex is a vulnerable region to early deposition of amyloid plaques, a key bio-marker in AD progression [28, 24]. Similarly, damage in the entorhinal, paracentral, frontal, and hippocampal structures are other early indicators of AD in studies of amyloid deposition and structural and functional MRI [14, 16, 31].

Additionally, we look at pattern frequency changes between groups at granular scale. Namely, we identify the most dominant pattern per node for each subject group that appears in at least half of the subjects. This is visualized in Fig. 5. Here, nodes in orange are those that have changed pattern, blue indicated no change, black had no definitive pattern within the control group, and labelled nodes are from Table 1.

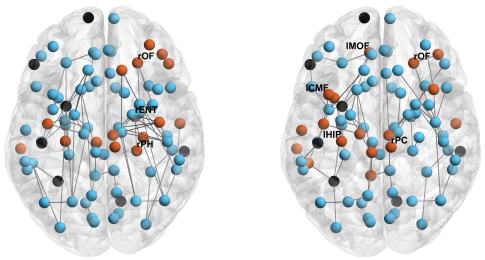

(a) Control vs. MCI (b) Control vs. MCIc

Fig. 5: Changes in pattern between healthy and disease. Note that only 2% of DTI edges are drawn for clarity. Generated with the BrainNet viewer tool [29].

5. CONCLUSION AND LIMITATIONS

We have extended the analysis of permutation patterns to graph signals, providing a novel lens to view and analyze such data at granular scale. Our findings indicate that the turning rate (α) and up-down balance (β) serve as effective tools for graph-based pattern analysis. Furthermore, we identify the potential use of graph based permutation patterns for multi-modal MRI data of MCI. Though limited by sample size, our results motivate larger studies of graph based permutation patterns on other real-world data such as MRI-based brain graph signals.

6. REFERENCES

[1] H. Azami and J. Escudero. Improved multiscale permutation entropy for biomedical signal analysis: Interpretation and application to electroencephalogram recordings. *Biomedical Signal Processing and Control*, 23:28–41, 2016.

[2] H. Azami, L. Faes, J. Escudero, et al. Entropy analysis of univariate biomedical signals: Review and comparison of methods. *Frontiers in Entropy across the Disciplines: Panorama of Entropy: Theory, Computation, and Applications*, pages 233–286, 2023.

[3] C. Bandt. Statistics and contrasts of order patterns in univariate time series. *Chaos*, 33(3), 2023.

[4] C. Bandt and B. Pompe. Permutation Entropy: A Natural Complexity Measure for Time Series. *Physical Review Letters*, 88(17):174102, apr 2002.

[5] C. Bandt and K. Wittfeld. Two new parameters for the ordinal analysis of images. *Chaos: An Interdisciplinary Journal of Nonlinear Science*, 33(4), 2023.

[6] C. Bastin and E. Delhaye. Targeting the function of the transentorhinal cortex to identify early cognitive markers of alzheimer's disease. *Cognitive, Affective, & Behavioral Neuroscience*, pages 1–11, 2023.

[7] A. Bessadok, M. A. Mahjoub, and I. Rekik. Graph neural networks in network neuroscience. *IEEE Transactions on Pattern Analysis and Machine Intelligence*, 45(5):5833–5848, 2022.

[8] C. R. Buchanan, C. R. Pernet, et al. Test–retest reliability of structural brain networks from diffusion mri. *Neuroimage*, 86:231–243, 2014.

[9] Y. Cao, W.-w. Tung, et al. Detecting dynamical changes in time series using the permutation entropy. *Physical review E*, 70(4):046217, 2004.

[10] M. Didic, E. J. Barbeau, O. Felician, E. Tramoni, E. Guedj, M. Poncet, and M. Ceccaldi. Which memory system is impaired first in alzheimer's disease? *Journal of Alzheimer's Disease*, 27(1):11–22, 2011.

[11] X. Dong, D. Thanou, L. Toni, M. Bronstein, and P. Frossard. Graph signal processing for machine learning: A review and new perspectives. *IEEE Signal processing magazine*, 37(6):117–127, 2020.

[12] J. S. Fabila-Carrasco, C. Tan, and J. Escudero. Permutation entropy for graph signals. *IEEE Transactions on Signal and Information Processing over Networks*, 8:288–300, 2022.

[13] J. S. Fabila-Carrasco, C. Tan, and J. Escudero. Dispersion entropy for graph signals. *Chaos, Solitons and Fractals*, 2023.

[14] A. M. Fjell, L. McEvoy, et al. What is normal in normal aging? Effects of aging, amyloid and Alzheimer's disease on the cerebral cortex and the hippocampus. *Progress in Neurobiology*, 117:20–40, jun 2014.

[15] W. Huang, T. A. Bolton, et al. A graph signal processing perspective on functional brain imaging. *Proceedings of the IEEE*, 106(5):868–885, 2018.

[16] M. P. Laakso, G. B. Frisoni, et al. Hippocampus and entorhinal cortex in frontotemporal dementia and Alzheimer's disease: a morphometric MRI study. *Biological Psychiatry*, 47(12):1056–1063, jun 2000.

[17] R. Li, X. Yuan, M. Radfar, P. Marendy, W. Ni, T. J. O'Brien, and P. M. Casillas-Espinosa. Graph signal processing, graph neural network and graph learning on biological data: a systematic review. *IEEE Reviews in Biomedical Engineering*, 16:109–135, 2021.

[18] F. C. Morabito, D. Labate, F. L. Foresta, A. Bramanti, et al. Multivariate multi-scale permutation entropy for complexity analysis of alzheimer's disease eeg. *Entropy*, 14(7):1186–1202, 2012.

[19] C. Morel and A. Humeau-Heurtier. Multiscale permutation entropy for two-dimensional patterns. *Pattern Recognition Letters*, 150:139–146, oct 2021.

[20] A. Ortega. *Introduction to graph signal processing*. Cambridge University Press, 2022.

[21] A. Ortega, P. Frossard, et al. Graph signal processing: Overview, challenges, and applications. *Proceedings of the IEEE*, 106(5):808–828, 2018.

[22] M. A. Parra, S. Abrahams, R. H. Logie, et al. Visual short-term memory binding deficits in familial Alzheimer's disease. *Brain*, 133(9):2702–2713, sep 2010.

[23] M. A. Parra, C. Calia, V. Pattan, and S. Della Sala. Memory markers in the continuum of the Alzheimer's clinical syndrome. *Alzheimer's Research and Therapy*, 14(1):1–16, dec 2022.

[24] S. M. Resnick, M. Lamar, and I. Driscoll. Vulnerability of the Orbitofrontal Cortex to Age-Associated Structural and Functional Brain Changes. *Annals of the New York Academy of Sciences*, 1121(1):562–575, dec 2007.

[25] M. Ribeiro, T. Henriques, L. Castro, et al. The entropy universe. *Entropy*, 23(2):222, 2021.

[26] M. Riedl, A. Müller, and N. Wessel. Practical considerations of permutation entropy: A tutorial review. *The European Physical Journal Special Topics*, 222(2):249–262, 2013.

[27] P. Scheltens, B. De Strooper, M. Kivipelto, et al. Alzheimer's disease. *The Lancet*, 397(10284):1577–1590, apr 2021.

[28] J. Sepulcre, M. R. Sabuncu, A. Becker, R. Sperling, and K. A. Johnson. In vivo characterization of the early states of the amyloid-beta network. *Brain*, 136(7):2239–2252, 2013.

[29] M. Xia, J. Wang, and Y. He. Brainnet viewer: a network visualization tool for human brain connectomics. *PloS one*, 8(7):e68910, 2013.

[30] Y. Yin and P. Shang. Weighted multiscale permutation entropy of financial time series. *Nonlinear Dynamics*, 78:2921–2939, 2014.

[31] Q. Zhao, H. Lu, et al. Evaluating functional connectivity of executive control network and frontoparietal network in Alzheimer's disease. *Brain Research*, 1678:262–272, jan 2018.

[32] L. Zunino, M. Zanin, B. M. Tabak, et al. Forbidden patterns, permutation entropy and stock market inefficiency. *Physica A*, 388:2854–2864, 2009.